

OPTIMAL DESIGN OF A SILICON-ON-INSULATOR NANOWIRE WAVEGUIDE FOR BROADBAND WAVELENGTH CONVERSION

X. Zhang, S. Gao, and S. He

Centre for Optical and Electromagnetic Research
State Key Laboratory of Modern Optical Instrumentation
Zhejiang University
Hangzhou 310058, China

Abstract—The broadband wavelength conversion based on four-wave mixing in a silicon nanowire waveguide is theoretically investigated by taking into account the influence of the waveguide loss and free-carrier absorption on the phase-matched condition. The lossy wavelength conversion is compared with the lossless one in terms of conversion efficiency and bandwidth. The size of the silicon-on-insulator nanowire waveguide is optimized to be $400\text{ nm} \times 269\text{ nm}$ for broadband wavelength conversion by realizing a flattened dispersion. The pump wavelength is also optimized to 1538.7 nm in order to further enhance the conversion bandwidth. A 3-dB conversion bandwidth of over 280 nm is achieved in the optimized waveguide with the optimized pump wavelength.

1. INTRODUCTION

With the development of the optical communication networks, all-optical signal processing including optical switching [1], wavelength conversion [2–6], optical amplification [7, 8], and signal regeneration [9] has attracted much attention. During the past few years silicon has emerged as an important material for all-optical signal processing since the relative low-cost fabrication process makes silicon-on-insulator (SOI) wafers an attractive and commercial platform for the integration of optical waveguides. The high index contrast of SOI waveguides allows for a tight confinement of optical waves to a sub-micron

Corresponding author: S. Gao (gaosm@zju.edu.cn).

region. Due to this ultra-small size and effective mode area, ultra-high intensities can be produced by the input optical powers at the milliwatt level. Moreover, SOI waveguides exhibit larger third-order nonlinearity than that of fibers in the telecommunication band [10]. These features enable efficient nonlinear phenomena to occur in the SOI waveguides. Many nonlinear effects, such as self-phase modulation (SPM) [11], cross-phase modulation (XPM) [12], four-wave mixing (FWM) and parametric amplification [2, 3, 8, 13, 14], two-photon absorption (TPA) [15], and stimulated Raman scattering (SRS) [16], have been demonstrated to efficiently occur with a relative low pump power in a short length of such waveguide. It opens a door for the SOI-based all-optical signal processing devices.

FWM, an important nonlinear parametric process conventionally used to realize wavelength conversion, parametric amplification, and signal regeneration, has been extremely concerned in SOI waveguides recently. FWM-based wavelength conversion was firstly demonstrated experimentally in straight SOI nanowire waveguides [2]. And then SOI waveguide-based high-Q microring resonators were also introduced in order to increase the conversion efficiency and decrease the pump power [17, 18]. The efficiency is tightly related to the effective mode area of the waveguide and some new structures such as slot waveguides [19, 20] and surface plasmon waveguides [21] have exhibited the ability to confine light. In addition, the dispersion of the SOI waveguides has been demonstrated to be governed by its shape and dimensions [22, 23], which provides the option to realize broadband wavelength conversion by tuning the dispersion characteristics of silicon nanowire waveguides [24]. Lin et al. reported the ultra-broadband wavelength conversion by tailoring the dispersion of waveguide under the consideration of the impact of the linear loss and absorptions [25], and Liu et al. introduced a dielectric film deposited around the silicon core for dispersion engineering to achieve a broadband FWM [26].

For FWM-based wavelength conversion, the conversion efficiency and bandwidth are also dominated by the phase-mismatch, which is determined by the dispersion of the SOI waveguides and the input pump powers [6]. Since the pump power will attenuate along the propagation distance in the SOI waveguides due to the loss and absorption, the phase-mismatch will be also dependent on them. In previous contributions, although the broadband wavelength conversion has been proposed [25, 26], the dependence of the phase-mismatch on the waveguide loss and absorption and the incident pump condition for the optimizing conversion response were still rarely investigated. In this paper, we mainly investigate the influence of the linear loss and free carrier absorption (FCA) on the phase-matched condition, and

optimize the SOI nanowire waveguide size and the incident pump to enhance the conversion bandwidth and efficiency. In Section 2, the theory of FWM is established by considering the linear loss and FCA, and a comparison between the lossy and lossless situations is made. In Section 3, the dispersion property depending on the geometric parameters of the SOI waveguide is investigated and the waveguide size is optimized in terms of the dispersion characteristics. Moreover, the incident pump wavelength is also optimized in order to enhance the conversion bandwidth in an optimized waveguide. Finally, a conclusion is drawn in Section 4.

2. THEORY

FWM is a nonlinear parametric process arising from the third-order nonlinearity. When a pump ω_p and a signal ω_s are injected into an SOI nanowire waveguide together, the degenerate FWM will efficiently occur and an idler $\omega_i = 2\omega_p - \omega_s$ will be efficiently generated once the phase-matched condition is satisfied. The degenerate FWM process is described by a set of coupled equations in terms of the complex field amplitudes of these waves:

$$\begin{aligned} \frac{dE_p(z)}{dz} = & \left[-\frac{\alpha_p}{2} - \frac{\sigma_p \beta_{TPA} \tau_{eff}}{4h_p c A_{eff}^2} \lambda_p |E_p(z)|^4 \right] E_p(z) \\ & + j\gamma_p \left[|E_p(z)|^2 + 2|E_s(z)|^2 + 2|E_i(z)|^2 \right] E_p(z) \\ & + j2\gamma_p E_p^*(z) E_s(z) E_i(z) \exp(j\Delta\beta z) \end{aligned} \quad (1)$$

$$\begin{aligned} \frac{dE_s(z)}{dz} = & \left[-\frac{\alpha_s}{2} - \frac{\sigma_s \beta_{TPA} \tau_{eff}}{4h_p c A_{eff}^2} \lambda_p |E_p(z)|^4 \right] E_s(z) \\ & + j\gamma_s \left[|E_s(z)|^2 + 2|E_p(z)|^2 + 2|E_i(z)|^2 \right] E_s(z) \\ & + j\gamma_s E_p^2(z) E_i^*(z) \exp(-j\Delta\beta z) \end{aligned} \quad (2)$$

$$\begin{aligned} \frac{dE_i(z)}{dz} = & \left[-\frac{\alpha_i}{2} - \frac{\sigma_i \beta_{TPA} \tau_{eff}}{4h_p c A_{eff}^2} \lambda_p |E_p(z)|^4 \right] E_i(z) \\ & + j\gamma_i \left[|E_i(z)|^2 + 2|E_p(z)|^2 + 2|E_s(z)|^2 \right] E_i(z) \\ & + j\gamma_i E_p^2(z) E_s^*(z) \exp(-j\Delta\beta z) \end{aligned} \quad (3)$$

where $E_{p,s,i}(z)$ are the complex field amplitudes of the pump, signal, and idler waves; $\alpha_{p,s,i}$ represent the linear propagation losses of the waveguide; $\sigma_{p,s,i}$ are the cross-sectional area of FCA; β_{TPA} is the coefficient of TPA; τ_{eff} is the carrier lifetime; h_p is the Planck constant;

c is the velocity of light in the vacuum; A_{eff} is the effective mode area of the waveguide; $\lambda_{p,s,i}$ are the wavelengths of the pump, signal and idler waves; $\gamma_{p,s,i}$ are the nonlinear parameters; and $\Delta\beta$ is the linear phase-mismatch, which is expressed as

$$\Delta\beta = \beta_s + \beta_i - 2\beta_p \quad (4)$$

where $\beta_{p,s,i}$ are the wave numbers of these interaction waves. Expanding $\beta_{p,s,i}$ in a Taylor series to the fourth-order around the pump wavelength λ_p , the linear phase-mismatch $\Delta\beta$ can be rewritten as

$$\begin{aligned} \Delta\beta = & -\frac{1}{2\pi c} \lambda_p^2 D(\lambda_p) \Omega^2 \\ & - \frac{1}{(2\pi c)^3} \left[\frac{1}{2} \lambda_p^4 D(\lambda_p) + \frac{1}{2} \lambda_p^5 D'(\lambda_p) + \frac{1}{12} \lambda_p^6 D''(\lambda_p) \right] \Omega^4 \end{aligned} \quad (5)$$

where $\Omega = \omega_s - \omega_p$ is the frequency difference between the pump and signal waves; $D(\lambda_p)$ is the dispersion parameter at the pump wavelength λ_p ; $D'(\lambda_p)$ and $D''(\lambda_p)$ are the first- and second-order derivatives of D at λ_p , respectively. When the pump wavelength is tuned near the zero-dispersion wavelength (ZDW), $D'(\lambda_p)$ and $D''(\lambda_p)$ play an important role in the phase-matched condition and a broad conversion bandwidth can be achieved.

Suppose that the pump is much stronger than the signal and idler, i.e., $P_p \gg P_{s,i}$, the SPM and XPM terms without the participation of the pump wave in Eqs (1)–(3). can be reasonably neglected. Since these involved waves are all in the conventional-band, the relatively small differences in the linear propagation losses, cross-sectional area of FCA and nonlinear parameters among them can be ignored, i.e., $\alpha_p = \alpha_s = \alpha_i = \alpha$, $\sigma_p = \sigma_s = \sigma_i = \sigma$, and $\gamma_p = \gamma_s = \gamma_i = \gamma = 2\pi n_2 / \lambda_p A_{eff}$. For convenience, the pump energy converted to the signal and idler waves can be neglected since it is much smaller than the power attenuation caused by the linear propagation loss and the FCA-induced loss of the waveguide. In this case, Eq. (1) can be simplified as

$$\frac{dE_p(z)}{dz} = -\frac{\alpha + \alpha_{FCA}}{2} E_p(z) + j\gamma |E_p(z)|^2 E_p(z) \quad (6)$$

where α_{FCA} is introduced to simplify the expression of the FCA-induced loss term and can be written as

$$\alpha_{FCA} = \frac{\sigma \beta_{TPA} \tau_{eff}}{2h_p c A_{eff}^2} \lambda_p P_{p0}^2 \quad (7)$$

where $P_{p0} = |E_p(0)|^2$ is the pump power. The pump distribution along the propagation distance in the waveguide can be analytically obtained by solving Eq. (6):

$$E_p(z) = \sqrt{P_{p0}} \exp\left(-\frac{\alpha + \alpha_{FCA}}{2}z\right) \exp\left[-j\frac{\gamma P_{p0} \exp(-(\alpha + \alpha_{FCA})z)}{\alpha + \alpha_{FCA}}\right] \quad (8)$$

Substituting Eq. (8) into Eqs. (2) and (3), the coupled equations can be rewritten as

$$\frac{dE_s(z)}{dz} = -\frac{\alpha + \alpha_{FCA}}{2}E_s(z) + j\gamma P_{p0} \exp[-(\alpha + \alpha_{FCA})z] \left\{ 2E_s(z) + E_i^*(z) \exp\left[-j\Delta\beta z - j\frac{2\gamma P_{p0} \exp(-(\alpha + \alpha_{FCA})z)}{\alpha + \alpha_{FCA}}\right] \right\} \quad (9)$$

$$\frac{dE_i^*(z)}{dz} = -\frac{\alpha + \alpha_{FCA}}{2}E_i^*(z) - j\gamma P_{p0} \exp[-(\alpha + \alpha_{FCA})z] \left\{ 2E_i^*(z) + E_s(z) \exp\left[j\Delta\beta z + j\frac{2\gamma P_{p0} \exp(-(\alpha + \alpha_{FCA})z)}{\alpha + \alpha_{FCA}}\right] \right\} \quad (10)$$

Using the transformation

$$E_m(z) = A_m(z) \exp\left[-\frac{(\alpha + \alpha_{FCA})z}{2} - j\frac{2\gamma P_{p0} \exp(-(\alpha + \alpha_{FCA})z)}{(\alpha + \alpha_{FCA})}\right] \quad (11)$$

Eqs. (9) and (10) can be rewritten as

$$\frac{dA_s(z)}{dz} = j\gamma P_{p0} \exp[-(\alpha + \alpha_{FCA})z] \exp\left[-j\Delta\beta z + j\frac{2\gamma P_{p0} \exp(-(\alpha + \alpha_{FCA})z)}{(\alpha + \alpha_{FCA})}\right] A_i^*(z) \quad (12)$$

$$\frac{dA_i^*(z)}{dz} = -j\gamma P_{p0} \exp[-(\alpha + \alpha_{FCA})z] \exp\left[j\Delta\beta z - j\frac{2\gamma P_{p0} \exp(-(\alpha + \alpha_{FCA})z)}{(\alpha + \alpha_{FCA})}\right] A_s(z) \quad (13)$$

From Eqs. (12) and (13), one can obtain the phase-mismatch of the involved waves:

$$\kappa(z) = \Delta\beta + 2\gamma P_{p0} \exp[-(\alpha + \alpha_{FCA})z] \quad (14)$$

where the first term on the right-hand-side of Eq. (14) is the linear phase-mismatch, and the second term represents the contribution of

the nonlinear effects to the phase-mismatch. As can be seen in Eq. (14), the phase-mismatch is dependent on the linear propagation loss and the FCA-induced loss, and it varies along the propagation distance.

The conversion efficiency η , which is defined as the ratio of the output idler power at $z = L$ to the input signal power at $z = 0$, can be expressed as

$$\eta = \frac{P_i(L)}{P_s(0)} \quad (15)$$

It can be numerically obtained by solving Eqs. (12) and (13) when the linear propagation loss and FCA are taken into account. While a lossless waveguide is considered ($\alpha = 0$ and $\alpha_{FCA} = 0$), the conversion efficiency can be written as the following expression by analytically solving Eqs. (12) and (13) [6]:

$$\eta = \left[\frac{\gamma P_p(0)}{g} \sinh(gL) \right]^2 \quad (16)$$

where $g = [(\gamma P_{p0})^2 - (\kappa/2)^2]^{1/2}$ is the parametric gain, and the phase-mismatch in this lossless case is

$$\kappa = \Delta\beta + 2\gamma P_{p0} \quad (17)$$

In this wavelength conversion process, the conversion efficiency is also related to the coherent length, which is defined as [6]

$$L_{coh} = \frac{\pi}{|\kappa|} \quad (18)$$

When the waveguide is longer than the coherent length, the energy will be converted from the signal to the pump and the efficiency will be decreased. Therefore, the waveguide dimensions should be selected under the condition of $L \leq L_{coh}$.

3. RESULTS AND DISCUSSION

The theoretical model under the lossless assumption in Section 2 was originally used to describe the FWM effect in optical fibers and it is transferred to describe that in silicon nanowire waveguides. It is quite accurate in optical fibers since fiber loss is small enough to be ignored. However, the situation in the SOI waveguides is different due to the relatively large propagation loss and FCA and the lossless assumption will introduce more deviation. Figure 1 shows the differences of the pump and idler waves along the propagation distance by considering the attenuation or not. The simulation results are obtained in a

250 nm \times 500 nm (height \times width) SOI waveguide for a TE-polarized pump wave of 200-mW input power at wavelength 1550 nm and a signal wave with the initial power of 1 mW at wavelength 1520 nm. Here the nonlinear index coefficient of silicon is supposed to be $6 \times 10^{-18} \text{ m}^2/\text{W}$; the effective mode area is $8.33 \times 10^{-2} \mu\text{m}^2$; and the nonlinear coefficient of the FWM process can be calculated as $2.92 \times 10^{-3} \text{ cm}^{-1}\text{mW}^{-1}$. Figs. 1(a) and 1(b) show the power evolution of the pump and idler waves in the lossless case, respectively. Under the undepleted pump approximation, the pump wave only acquires a phase shift while the power maintains unchanged, as shown in Fig. 1(a). The oscillation of the idler power along the propagation distance shown in Fig. 1(b) indicates the energy conversion between the pump and idler waves. The phase-mismatch of the involved waves is about -0.68 cm^{-1} in the case of 30-nm detuning and the coherent length L_{coh} is about 4.6 cm according to Eq. (18). Within this length, the power flows from the pump to the signal and idler waves. While in Figs. 1(c) and 1(d), the parameter values used in the simulation are supposed as: $\alpha = 2.5 \text{ dB/cm}$, $\sigma = 1.45 \times 10^{-17} \text{ cm}^2$, $\beta_{TPA} = 0.3 \text{ cm/GW}$, and $\tau_{eff} = 1 \text{ ns}$, and these values are used in the simulation all through

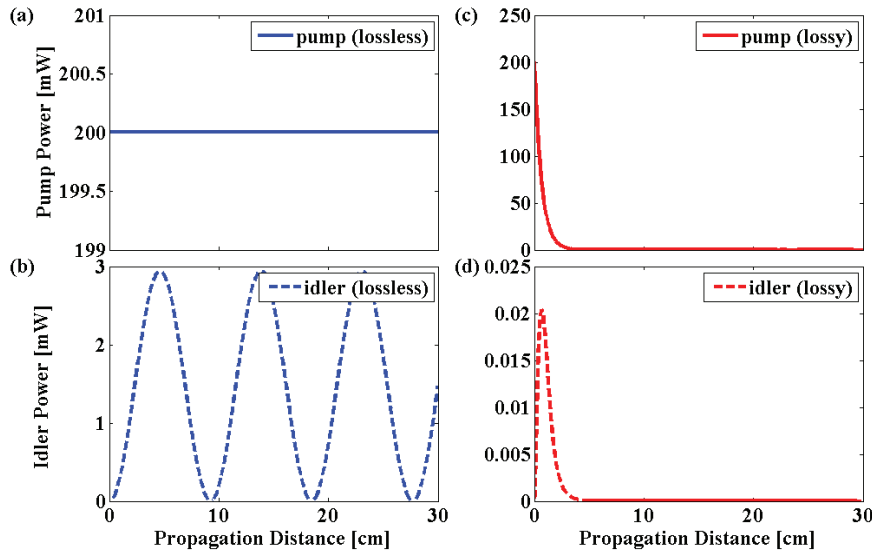


Figure 1. Evolution of the pump and idler waves along the propagation distance. (a) Pump evolution in the lossless case; (b) idler evolution in the lossless case; (c) pump evolution in the lossy case; (d) idler evolution in the lossy case.

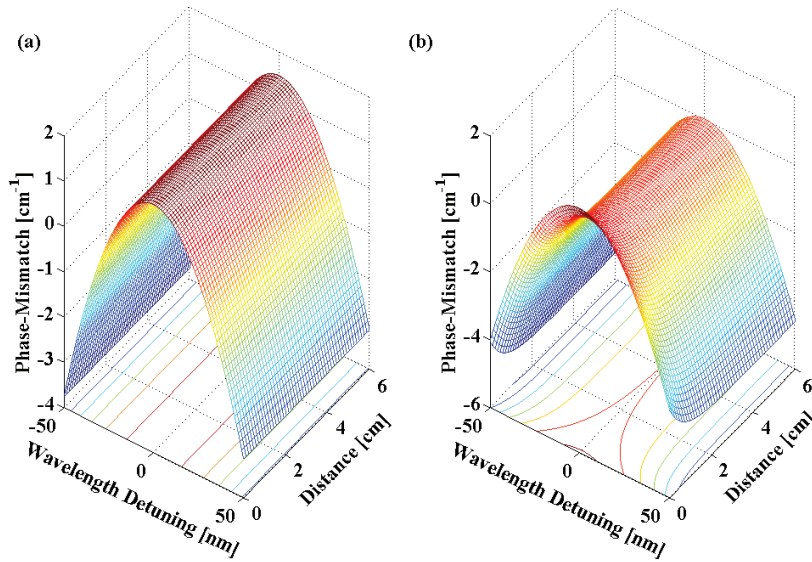


Figure 2. Phase-mismatch as a function of the wavelength detuning and propagation distance in (a) lossless and (b) lossy cases.

this paper. As shown in Fig. 1(c), the pump wave attenuates rapidly within a short distance. And as can be seen in Fig. 1(d), the peak value of the idler wave is much smaller than that in the lossless case [see in Fig. 1(b)] and the location of this peak emerges much earlier in the waveguide.

The conversion bandwidth and efficiency are determined by the phase-mismatch which is related to the linear propagation loss and the FCA-induced loss of the waveguides, as described in Eq. (14). Fig. 2 shows the phase-mismatch κ as a function of the wavelength detuning $\lambda_s - \lambda_p$ and the propagation distance z in a $250 \text{ nm} \times 500 \text{ nm}$ waveguide. The pump wave used here is the same as that in Fig. 1 and the signal wave is scanned within a wavelength range of 100 nm around the pump. Fig. 2(a) shows the phase-mismatch of the involved waves in the lossless case. The phase-mismatch maintains unchanged while propagating through the waveguide. The loss-dependent phase-mismatch is shown in Fig. 2(b). When the waves propagate along the waveguide, a decrease of the phase-mismatch is introduced by the pump attenuation due to the propagation loss and FCA. Thus, the phase-matched condition is no longer satisfied during the propagation of the waves even if the pump and signal waves are placed at the phase-matched locations at the input port ($z = 0$). Since the phase-matched

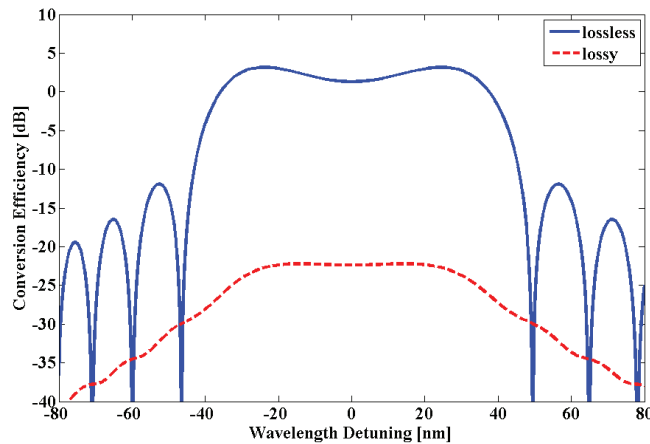


Figure 3. Conversion efficiency as a function of the wavelength detuning in the lossless (solid line) and lossy (dashed line) cases.

condition can not be held in real lossy waveguides, the conversion efficiency drops and the conversion bandwidth becomes narrower than that in the lossless case. Fig. 3 shows the conversion efficiency as a function of the wavelength detuning in the waveguide mentioned above in both the lossless and lossy cases and the pump wavelength and input power are the same as those in Fig. 1. The waveguide length is 2 cm which is shorter than the coherent length. Compared with the real lossy case (dashed curve), the conversion efficiency and the 3-dB conversion bandwidth under the lossless assumption (solid curve) are about 25 dB and 5 nm over-evaluated. Therefore, the lossy model will be used in the following analysis.

Since the dispersion property of the waveguide determines the linear phase-mismatch of the involved waves, it is tightly related to the conversion efficiency and bandwidth. The linear phase-mismatch can be considered as the contribution of two parts: One is the material dispersion, which is large and normal within the wavelength range we are interested in. And the other is the waveguide dispersion, which can be varied from anomalous to normal by adjusting the waveguide dimensions [22]. Fig. 4 shows the values of ZDW corresponding to different waveguide sizes, where the width and height of the waveguide core are scanned with a step of 25 nm. Generally, there are two ZDWs in the entire wavelength region and both of them shift to the long wavelength for TE mode as the waveguide dimensions increase. For TM mode, the left ZDW shifts first to the short and then to the long wavelength and the right ZDW keeps increasing as the waveguide

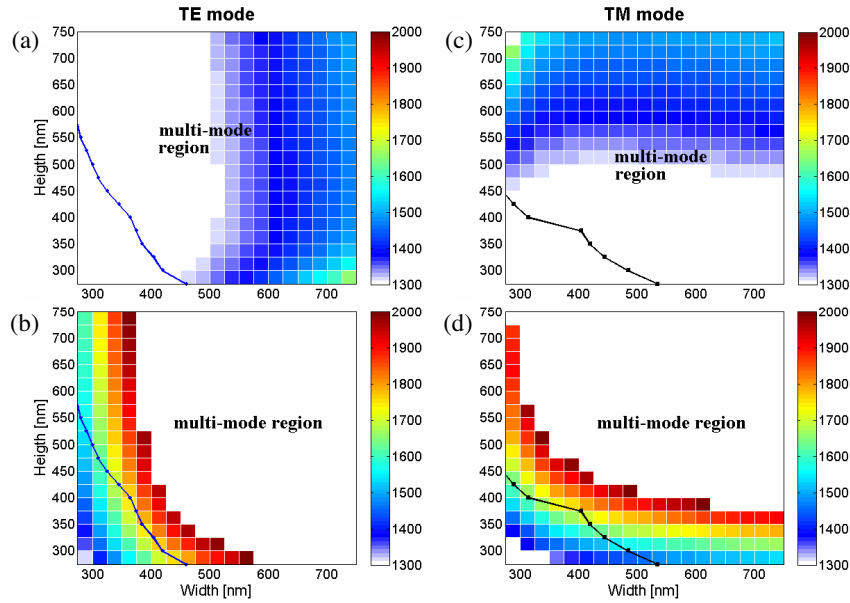


Figure 4. Distribution of the ZDWs for the TE and TM modes. (a) The left ZDW for TE mode; (b) the right ZDW for TE mode; (c) the left ZDW for TM mode; (d) the right ZDW for TM mode. The solid lines in (a)–(d) denote the single-mode conditions for TE or TM modes.

dimensions increase. Figs. 4(a) and 4(b) show the distribution of the left and the right ZDWs for TE mode in terms of the waveguide dimensions, respectively. Figs. 4(c) and 4(d) are for TM mode. The available wavelength range is considered from 1300 to 2000 nm (shown as the colorful zone in Fig. 4). The white zone in Fig. 4 indicates that there is no ZDW within this wavelength range.

In order to avoid the influence of higher-order modes on the FWM process, the nanowire waveguide is required to be of single mode. The propagation characteristics in the waveguides can be analyzed by various computational methods [27–29], e.g., the finite-difference time-domain (FDTD) method [30,31] and the beam propagation method (BPM) [32]. In this paper, the single-mode condition for the waveguides at a specific wavelength of 1550 nm is numerically analyzed by using the semi-vectorial BPM. To obtain the single-mode condition, one can scan the height and width of the silicon waveguide and judge whether the higher-order modes exist. For a fixed height we

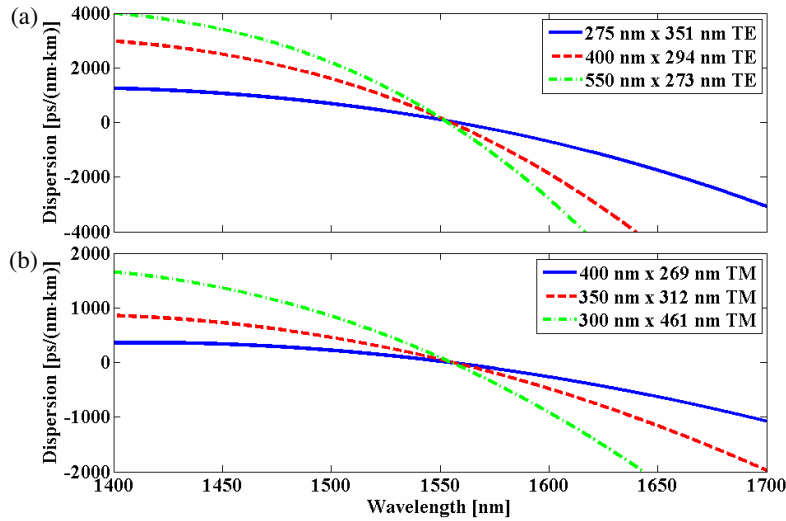


Figure 5. Dispersion as a function of the wavelength for (a) TE and (b) TM modes.

reduce the width with a step of 5 nm until all the higher-order modes disappear. The calculated results are also shown in Fig. 4. The solid curves indicate the critical boundaries of single mode for TE mode in Figs. 4(a) and 4(b), and the curves are for TM mode in Figs. 4(c) and 4(d). The single-mode region is on the left-bottom side of the curve and the multi-mode region is on the right-top side in each figure.

The previous research has demonstrated that a broader conversion bandwidth will be achieved when placing the pump wave in the anomalous region of the waveguide, since the positive nonlinear phase-mismatch can be compensated by the induced negative linear phase-mismatch [6]. From Fig. 4, for a certain ZDW such as 1555 nm, one can find a series of waveguides which satisfy the requirement under the single-mode condition. Fig. 5 shows the dispersion parameter D as a function of the wavelength for some waveguides whose ZDWs are all around 1555 nm. As shown in Fig. 5(a), for TE mode the dispersion slope increases as the height of waveguide increases. The situation is reversed for TM mode in Fig. 5(b). The flatter the curve is, the broader the conversion bandwidth is because the phase-mismatch of the involved waves maintains small values within a wide wavelength range. After comparing the dispersion slopes of these waveguides, the waveguide cross section is optimized as 400 nm \times 269 nm for TM mode in order to obtain the smallest dispersion slope that corresponds to the

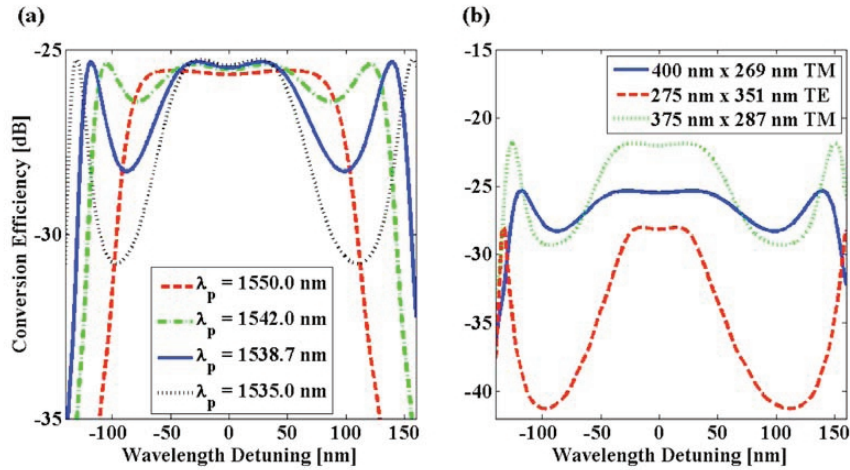


Figure 6. (a) Conversion efficiency as a function of the wavelength detuning for different pump wavelengths in the optimized 400 nm \times 269 nm waveguide; (b) Conversion response comparison of the 400 nm \times 269 nm (solid line), 275 nm \times 351 nm (dashed line), and 375 nm \times 287 nm (dotted line) waveguides with the optimized pump wavelength.

broadest conversion bandwidth.

The conversion bandwidth is also related to the pump wavelength and power since the loss-dependent phase-mismatch is quite related to them. The bandwidth can be enhanced by properly adjusting the pump wavelength at a fixed input pump power. Figure 6(a) shows the conversion response, that is, the conversion efficiency versus the wavelength detuning, for different pump wavelengths in the anomalous region in the optimized waveguide of 400 nm \times 269 nm with a fixed input power of 200 mW. The nonlinear phase-mismatch introduces a depression of the conversion efficiency near the pump and a broad phase-matched region with two peaks on both sides of the pump appears (dashed line). When the pump is tuned away from the ZDW, the appearance of a second pair of conversion efficiency peaks farther from the pump, which is introduced by the location shift and number increase of the perfect phase-matched wavelengths, increases the 3-dB conversion bandwidth (dash-dot and solid lines). And the sharp drop of more than 3-dB between the first and second peaks limits the increase of the 3-dB conversion bandwidth when further tuning the pump wave away from the ZDW (dotted line). As shown in Fig. 6(a), the maximum conversion bandwidth is achieved when pumping at 1538.7 nm (solid

line) under the assumption of 200-mW input pump power and 2-cm-long interaction length.

To demonstrate the optimization results, Fig. 6(b) simulates the conversion response for the optimized waveguide of $400\text{ nm} \times 269\text{ nm}$ for TM polarization together with two other waveguides with the dimensions of $275\text{ nm} \times 351\text{ nm}$ for TM polarization and $375\text{ nm} \times 287\text{ nm}$ for TM polarization for comparison. These results are obtained in a 2-cm-long waveguide with a 200-mW pump wave at 1538.7 nm. The coherent length of the optimized waveguide is about 2 cm for a wavelength detuning of $|\lambda_s - \lambda_p| \approx 120\text{ nm}$. The 3-dB conversion bandwidth is over 280 nm for the optimized waveguide and the bandwidths of $275\text{ nm} \times 351\text{ nm}$ and $375\text{ nm} \times 287\text{ nm}$ waveguides are about 77 nm and 112 nm, respectively. As can be seen in Fig. 6(b), an ultra-broad 3-dB conversion bandwidth is achieved in the optimized waveguide with the optimized pump wavelength.

4. CONCLUSIONS

The FWM-based broadband wavelength conversion in silicon nanowire waveguides has been theoretically investigated. The theoretical analysis is performed by taking the waveguide propagation loss and FCA into account and compared with the lossless one. The dimensions of the SOI nanowire waveguides are optimized in terms of the dispersion for conversion bandwidth enhancement. Meanwhile, the pump wavelength is also optimized in order to enhance the conversion bandwidth further. Under these optimized conditions, a 3-dB conversion bandwidth of over 280 nm is achieved in the $400\text{ nm} \times 269\text{ nm}$ waveguide with a pump at wavelength 1538.7 nm.

ACKNOWLEDGMENT

This work is supported in part by the National Natural Science Foundation of China (Grant Nos. 60708006 and 60688401) and the Specialized Research Fund for the Doctoral Program of Higher Education of China (Grant No. 20070335118).

REFERENCES

1. Moghimi, M. J., H. Ghafoori-Fard, and A. Rostami, "Analysis and design of all-optical switching in apodized and chirped Bragg gratings," *Progress In Electromagnetics Research B*, Vol. 8, 87–102, 2008.

2. Fukuda, H., K. Yamada, T. Shoji, M. Takahashi, T. Tsuchizawa, T. Watanabe, J.-I. Takahashi, and S.-I. Itabashi, "Four-wave mixing in silicon wire waveguides," *Opt. Express*, Vol. 13, No. 12, 4629–4637, 2005.
3. Rong, H., Y.-H. Kuo, A. Liu, M. Paniccia, and O. Cohen, "High efficiency wavelength conversion of 10 Gb/s data in silicon waveguides," *Opt. Express*, Vol. 14, No. 3, 1182–1188, 2006.
4. Kuo, Y.-H., H. Rong, V. Sih, S. Xu, M. Paniccia, and O. Cohen, "Demonstration of wavelength conversion at 40 Gb/s data rate in silicon waveguides," *Opt. Express*, Vol. 14, No. 24, 11721–11726, 2006.
5. Yamada, K., H. Fukuda, T. Tsuchizawa, T. W. A.-T. Watanabe, T. S. A.-T. Shoji, and S. I. A.-S. Itabashi, "All-optical efficient wavelength conversion using silicon photonic wire waveguide," *IEEE Photon. Tech. Lett.*, Vol. 18, No. 9, 1046–1048, 2006.
6. Foster, M. A., A. C. Turner, R. Salem, M. Lipson, and A. L. Gaeta, "Broad-band continuous-wave parametric wavelength conversion in silicon nanowaveguides," *Opt. Express*, Vol. 15, No. 20, 12949–12958, 2007.
7. Rostami, A. and A. Salmanogli, "Investigation of light amplification in Si-nanocrystal-Er doped optical fiber," *Progress In Electromagnetics Research B*, Vol. 9, 27–51, 2008.
8. Foster, M. A., A. C. Turner, J. E. Sharping, B. S. Schmidt, M. Lipson, and A. L. Gaeta, "Broad-band optical parametric gain on a silicon photonic chip," *Nature*, Vol. 441, No. 7096, 960–963, 2006.
9. Salem, R., M. A. Foster, A. C. Turner, D. F. Geraghty, M. Lipson, and A. L. Gaeta, "Signal regeneration using low-power four-wave mixing on silicon chip," *Nature Photon.*, Vol. 2, No. 1, 35–38, 2008.
10. Lin, Q., O. J. Painter, and G. P. Agrawal, "Nonlinear optical phenomena in silicon waveguides: Modeling and applications," *Opt. Express*, Vol. 15, No. 25, 16604–16644, 2007.
11. Boyraz, O., T. Indukuri, and B. Jalali, "Self-phase-modulation induced spectral broadening in silicon waveguides," *Opt. Express*, Vol. 12, No. 5, 829–834, 2004.
12. Hsieh, I. W., X. G. Chen, J. I. Dadap, N. C. Panoiu, R. M. Osgood, S. J. Mcnab, and Y. A. Vlasov, "Cross-phase modulation-induced spectral and temporal effects on co-propagating femtosecond pulses in silicon photonic wires," *Opt. Express*, Vol. 15, No. 3, 1135–1146, 2007.

13. Espinola, R., J. Dadap, J. R. Osgood, S. McNab, and Y. Vlasov, "C-band wavelength conversion in silicon photonic wire waveguides," *Opt. Express*, Vol. 13, No. 11, 4341–4349, 2005.
14. Raghunathan, V., R. Claps, D. Dimitropoulos, and B. Jalali, "Parametric Raman wavelength conversion in scaled silicon waveguides," *J. Lightwave Technol.*, Vol. 23, No. 6, 2094–2102, 2005.
15. Tsang, H. K., C. S. Wong, T. K. Liang, I. E. Day, S. W. Roberts, A. Harpin, J. Drake, and M. Asghari, "Optical dispersion, two-photon absorption and self-phase modulation in silicon waveguides at 1.5 μm wavelength," *Appl. Phys. Lett.*, Vol. 80, No. 3, 416–418, 2002.
16. Liu, A. S., H. S. Rong, and M. Paniccia, "Net optical gain in a low loss silicon-on-insulator waveguide by stimulated Raman scattering," *Opt. Express*, Vol. 12, No. 18, 4261–4268, 2004.
17. Turner, A. C., M. A. Foster, A. L. Gaeta, and M. Lipson, "Ultra-low power parametric frequency conversion in a silicon microring resonator," *Opt. Express*, Vol. 16, No. 7, 4881–4887, 2008.
18. Liu, L., J. van Campenhout, G. Roelkens, D. van Thourhout, P. Rojo-Romeo, P. Regreny, C. Seassal, J. M. Fedeli, and R. Baets, "Ultralow-power all-optical wavelength conversion in a silicon-on-insulator waveguide based on a heterogeneously integrated III-V microdisk laser," *Appl. Phys. Lett.*, Vol. 93, No. 06, 001107-1–061107-3, 2008.
19. Almeida, V. R., Q. Xu, C. A. Barrios, and M. Lipson, "Guiding and confining light in void nanostructure," *Opt. Lett.*, Vol. 29, No. 11, 1209–1211, 2004.
20. Baehr-Jones, T., M. Hochberg, C. Walker, and A. Scherer, "High-Q optical resonators in silicon-on-insulator-based slot waveguides," *Appl. Phys. Lett.*, Vol. 86, No. 08, 081101-1-081101-3, 2005.
21. Liu, L., Z. Han, and S. He, "Novel surface plasmon waveguide for high integration," *Opt. Express*, Vol. 13, No. 17, 6645–6650, 2005.
22. Turner, A. C., C. Manolatou, B. S. Schmidt, M. Lipson, M. A. Foster, J. E. Sharping, and A. L. Gaeta, "Tailored anomalous group-velocity dispersion in silicon channel waveguides," *Opt. Express*, Vol. 14, No. 10, 4357–4362, 2006.
23. Lamont, M. R. E., B. T. Kuhlmeier, and C. M. de Sterke, "Multi-order dispersion engineering for optimal four-wave mixing," *Opt. Express*, Vol. 16, No. 10, 7551–7563, 2008.
24. Zhang, X., S. Gao, and S. He, "Optimal design of silicon-

- on-insulator nano-wire waveguides for broadband wavelength conversion,” *Proceedings of Asia Optical Fiber Communications and Optoelectronic Conference*, paper SaN5, Shanghai, China, October 2008.
25. Lin, Q., J. Zhang, P. M. Fauchet, and G. P. Agrawal, “Ultrabroadband parametric generation and wavelength conversion in silicon waveguides,” *Opt. Express*, Vol. 14, No. 11, 4786–4799, 2006.
 26. Liu, X., W. M. Green, X. Chen, I-W. Hsieh, J. I. Dadap, Y. A. Vlasov, and R. M. Osgood, Jr., “Conformal dielectric overlayers for engineering dispersion and effective nonlinearity of silicon nanophotonic wires,” *Opt. Lett.*, Vol. 33, No. 24, 2889–2891, 2008.
 27. Rostami, A. and H. Motavali, “Asymptotic iteration method: A powerful approach for analysis of inhomogeneous dielectric slab waveguides,” *Progress In Electromagnetics Research B*, Vol. 4, 171–182, 2008.
 28. Samuel, E. P. and D. S. Patil, “Analysis of wavefunction distribution in quantum well biased laser diode using transfer matrix method,” *Progress In Electromagnetics Research Letters*, Vol. 1, 119–128, 2008.
 29. Hatamzadeh-Varmazyar, S. and M. Naser-Moghadasi, “New numerical method for determining the scattered electromagnetic fields from thin wires,” *Progress In Electromagnetics Research B*, Vol. 3, 207–218, 2008.
 30. Chu, S. T. and S. K. Chaudhuri, “Finite-difference time-domain method for optical waveguide analysis,” *Prog. Electromagn. Res.*, Vol. 11, 255–300, 1995.
 31. Hernandez-Lopez, M. A. and M. Quintillan, “Propagation characteristics of modes in some rectangular waveguides using the finite-difference time-domain method,” *J. Electromagn. Waves Appl.*, Vol. 14, No. 12, 1707–1722, 2000.
 32. Xu, C. L. and W. P. Huang, “Finite-difference beam propagation method for guide-wave optics,” *Prog. Electromagn. Res.*, Vol. 11, 1–49, 1995.